Available online at www.CivileJournal.org

Civil Engineering Journal

(E-ISSN: 2476-3055; ISSN: 2676-6957)

Vol. 7, No. 03, March, 2021

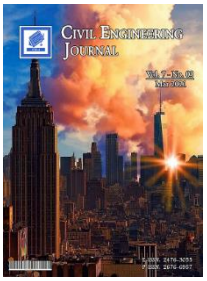

Inelastic Analysis of Mdof Systems Damaged by Earthquakes, Posteriorly Subjected to Wind Load

Oualid Badla [1*], T. Bouzid [1], P Martinez Vazquez [2]

[1] *Department of Civil Engineering, University of Batna 2, Batna 05000, Algeria.*

[2] *School of Engineering, University of Birmingham, B15 2TT, United Kingdom.*

Received 15 November 2020; Revised 09 February 2021; Accepted 15 February 2021; Published 01 March 2021

Abstract

This paper deals with the analysis of the inelastic response of buildings originally damaged by earthquakes and subjected to earthquake aftershock and wind loading. The overall aim is to establish the effect of wind actions on structural stability. To that end, one four-story bare frame benchmarked by the European Laboratory for Structural Assessment, is subject to various levels of winds and earthquake joint load while monitoring changes on the ductility demand. In this paper is shown that the combined action of strong winds and earthquakes, however its low probability of occurrence, would cause a decrease of strength reduction factors and considerably increase the ductility demand of damaged infrastructure hence inducing additional risks that would otherwise remain unquantified. The paper examines the non-linear performance of Multi-degree of freedom systems subject to various levels of winds and earthquake load and deals with the estimation of strength reduction factors. This is a relatively unexplored area of research which builds on past developments whereby inelastic performance of buildings has been discussed. It also links to various other paths of development such as structural reliability, forensic and control systems engineering.

Keywords: Ductility Demands; Seismic Engineering; Wind Load & Aerodynamics; RC Frame Elements; Far-fault Earthquakes; Near-fault Earthquakes.

1. Introduction

Most structures designed according to current code provisions will sustain damage in the event of a design-level earthquake occurrence, which to a good extent, is expected. It is well known that structural damage is directly related to ductility demands [1] and therefore evaluation of their relationship is very important for accurately assessing structural performance. Past research shows that current design standards for seismic design and seismic assessment, can improve significantly through the explicit account of ductility demands [2].

The evaluation of ductility demands for structures is abundantly reported in past research, see for example Yi et al. (2007) study [2]. According to these, the extreme design values of ductility relate to rare events. Earthquake design of structures generally allows for inelastic deformation depending on the target performance level. Proper structural performance thus relies on inelastic deformations that correspond to expected ductility or drift levels.

The structural demand due to an earthquake ground motion can be approximated by performing nonlinear time history analyses with computational models subject to a given ground motion. However, it seems appropriate not only

* Corresponding author: badla.oualid@univ-khenchela.dz

http://dx.doi.org/10.28991/cej-2021-03091675

consider isolated 'design earthquakes' but take one step forward to account for the inelastic response of buildings originally damaged by earthquakes that are subject to moderate or strong aftershocks. In such scenarios, if not during the original design, once can assume that wind is flowing. This depict multi-hazard scenarios not been studied in the past. To the authors' knowledge, only a few studies have examined the aftershocks effects on buildings while only a few revised combined earthquake and wind joint load. Moreover, to date some studies still report on simplified modelling techniques that omit integrating hysteretic beam or column behavior. Hatzigeorgiou and Beskos (2009) and Hatzigeorgiou (2010) [3, 4] focused on the response of Single-of-Degree-Of-Freedom (SDOF) systems assuming bilinear elastoplastic hysteresis with no stiffness and strength degradation. MDOF systems can more efficiently integrate beams, columns, and beam–column joints that can be deform in different manners due to cyclic loading reversals propagated by earthquake ground motion. It is to note that, global ductility depends on inter-story drift at higher rates that it does on roof drift [5]. Hysteretic models with stiffness degradation better simulate peak displacement of short period of structures than those assuming non-degrading hysteresis behavior [6].

Chopra and Chintanapakdee (2001) [7] studied far-fault and near-fault ground motions to determine qualitative differences on structural performance. That study showed that near-fault motions tend to induce greater displacement demand than far-fault motions in the constant acceleration region. This is apparently due to the fact that for near-fault ground motions, the average corner period (the period at which the constant velocity region begins) of the response spectra shifts to longer periods. The constant velocity region for near-fault motions is also generally narrower than that of far-fault motions.

All these studies assume, however, that earthquake and wind events are uncorrelated. This assumption seems reasonable when accepting that the structure's lifetime assumed for either design condition does limit their joint probability of occurrence. However little to no research has been produced for cases in which major earthquake events clash with low to moderate winds whose probability of occurrence is significant or when notwithstanding its low probability of occurrence, major seismic and wind events coincide. The latter does not seem unlikely after all if we consider the number of aftershocks that usually follow major earthquake events. For example, the earthquake that hit Nepal in 2015 (Ms =7.8) killing more than 8,000 [8] was followed by 30 aftershocks of Ms < 5 occurring within three weeks and killing 200 more. The earthquake that hit the Sichuan Province in China in 2008 (Ms =7.9) killing over 87,000 [9] was followed by 12 weeks with 42 aftershocks ranging in magnitude between 5 < Ms < 6.4. If we add this to the fact that wind is constantly flowing with a minimum speed that is equal to the average local wind velocity, then the current design assumptions concerning the unrelated action of wind and earthquakes do not seem conservative [10]. It thus appears that new research avenues generate through consideration of near- or far-fault earthquake events followed by moderate to strong aftershocks that occur simultaneously to wind actions .This paper attempts to address this knowledge gap through the estimation of ductility demands (μ) of structures subject to the combined effect of earthquake and wind load. The latter, flowing at mean speeds ranging between 5 ms^{-1} and 50 ms^{-1}. The subject of the investigation is the four-story bare frame standardized by the European Laboratory for Structural Assessment (ELSA) [11, 12]. This building is thus subject to multiple near- and far-fault seismic ground motions. The structural response is assessed by nonlinear dynamic (time history) analysis, to estimate the overall response.

This paper is organized mainly in different sections. The introduction portion is followed by an overview of the ductility demand, the structure configuration and material properties. Then the seismic input, wind filed simulation, wind and earthquake loading, which is followed by the results of the combined effect of earthquake and wind load. The latter, flowing at mean speeds ranging between 5 ms^{-1} and 50 ms^{-1} is conducted to obtain expressions for the ductility demands, in terms of the force reduction factor, and finally, conclusions and recommendations are provided.

2. Ductility Demand: An Overview

An adequate design is accomplished when a structure is dimensioned and detailed in such a way that the local (story and member) ductility demands are smaller than their corresponding capacities. Thus, during the preliminary design of a structure, there is a need to estimate the lateral strength (lateral load capacity) of the structure that is required in order to limit the global (structure displacement) ductility demand to a certain pre-determined value, which results in adequate prediction of localized damage.

The inelastic deformation experienced by a system under a given ground motion can be determined through the displacement ductility ratio, μ, which is defined as the ratio of maximum absolute relative displacement to its yield displacement this definition is given by Miranda (1993) [13].

$$\mu=\frac{umax-inelastic}{u_y} \quad (1)$$

The governing equation for SDOF inelastic system subjected to horizontal ground acceleration ü (t) is

$$m\ddot{u}(t)+c\dot{u}(t)+f_s(u,\dot{u})=-m\ddot{u}_g(t) \quad (2)$$

For a given excitation $\ddot{u}_g(t)$, the deformation $u(t)$ depends on three systems parameters: ω_n, ζ, and u_y, in addition to the form of the force-deformation relation. This becomes evident if Equation 2 is divided by m to obtain:

$$\ddot{u} + 2\zeta\omega_n\dot{u} + \omega_n^2 u_y \tilde{f}_s(u, \dot{u}) = -\ddot{u}_g(t) \quad (3)$$

Where $\omega_n$is the natural vibration frequency, $T_n = {2\pi}/{\omega_n}$ is the natural vibration period, and ζ is the damping ratio of the system vibrating within its linear elastic range (i.e., $u \leq u_y$). Equation 3 is rewritten in terms of $\mu(t) = u(t)/u_y$in order to identify the parameters that influence the ductility factor μ, Equation 1, the peak value of $\mu(t)$. Substituting $u(t) = u_y\,\mu(t)$, $\dot{u}(t) = u_y\,\dot{\mu}(t)$, $\ddot{u}(t) = u_y\,\ddot{\mu}(t)$ in Equation 3 and dividing by u_y gives:

$$\ddot{\mu} + 2\zeta\omega_n\dot{\mu} + \omega_n^2 \tilde{f}_s(u, \dot{u}) = -\omega_n^2 \frac{\ddot{u}_g(t)}{a_y} \quad (4)$$

Where $a_y = f_y/m$ may be interpreted as the acceleration of the mass required to produce the yield force f_y.

For given $\ddot{u}_g(t)$, μ depends on three system parameters: ω_n,ζ_y, R_y [Chopra, 2001]. The maximum force response of a linear elastic system can be denoted by f_{el}, while the yield strength of a nonlinear elasto-plastic system can be denoted by f_y. Thus, the force reduction R factor can be defined as

$$R_\mu = \frac{f_{el(\mu=1)}}{f_{y(\mu=\mu)}} \quad (5)$$

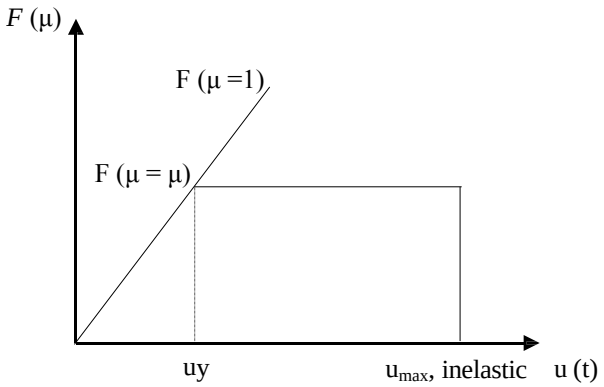

Figure 1. Illustrates the transition from elastic to plastic behaviour of one sdof oscillator

This method has been widely used to determine inelastic response spectra considering at least three non-linear load-deformation models: elastoplastic, bilinear, and stiffness degrading – see for example Miranda and Bertero (1994), Chopra and Goel (1999), and Riddell et al. (2002) [14-16]. In the present research the elastoplastic model is adopted.

3. Structural Configuration and Material Characteristics

The present study adopts the four-story reinforced concrete prototype shown in Figure 2. The concrete frame has been tested at the European Laboratory for Structural assessment (ELSA) [11, 12] under two subsequent pseudo-dynamic loadings. The two reinforced concrete frames tested at (ELSA) laboratory can be considered representative of the design and construction common practice until the late 1970's in southern European countries such as Italy, Portugal and Greece. They were designed to primarily withstand vertical loads such that its lateral resistance is of 5% of the frame weight [12]. The reinforcement details were specified in accordance to the normative available and to the construction practice at that time. Thus, no specific seismic detailing provisions were considered, preferential inelastic dissipation mechanisms were not assumed and no specific ductility or strength provisions were provided.

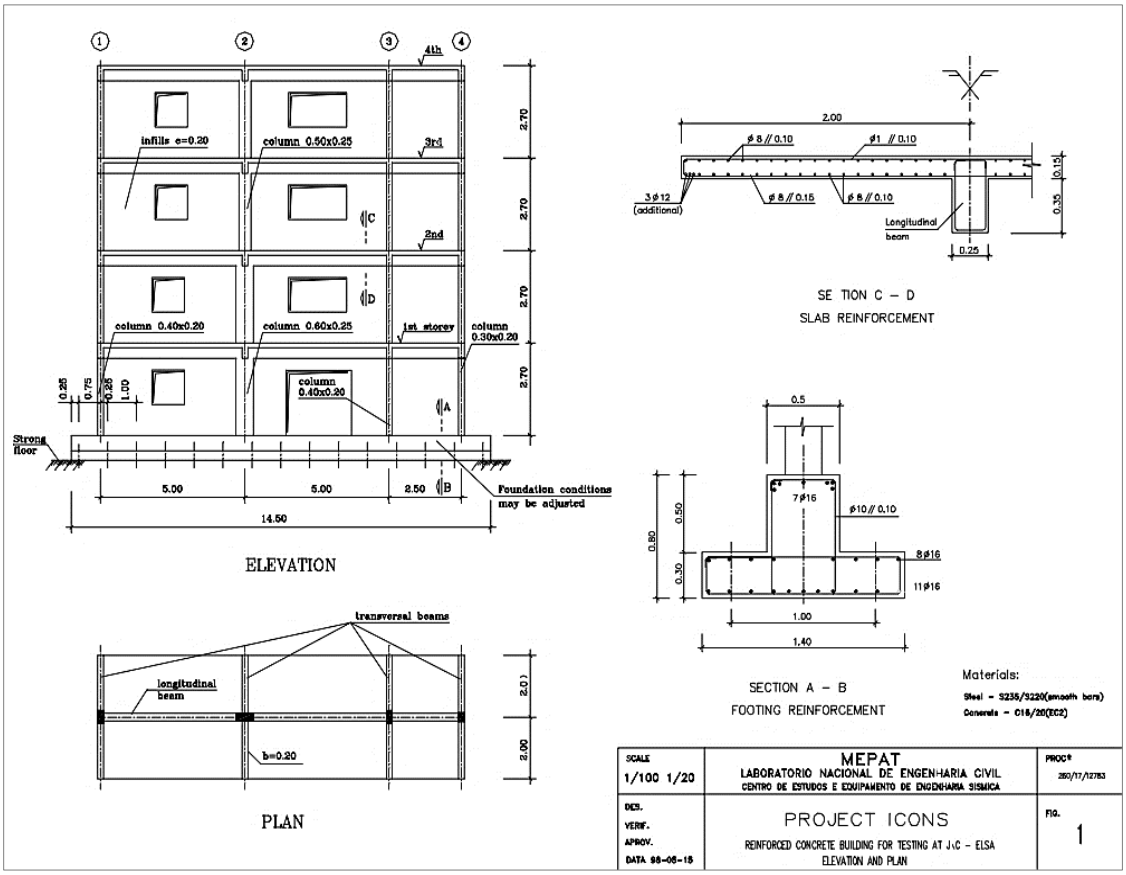

Figure 2. Four-story, three-bay RC frame geometry (m), (elevation and plan views [12]

The vertical loads, represented in Figure 3, were defined in order to simulate the dead load other than the self-weight of the frame, considering that parallel frames have a distance of 5.0 m Carvalho et al. (1999) [12]. The frame model includes a 4.0 m wide slab, which requires additional vertical load accounting for such a slab portion missing. Vertical distributed loads on beams and concentrated loads on the column were considered in order to simulate the dead load of the frame other than the weight of partitions, finishings and live load The distribution of vertical loads applied to the infilled frame to simulate the dead load other than the self-weight of the frame was identical to the one used for the bare frame, and imposing the same load distribution for all the tests. The scheme of the loads considered can be found in Pinto et al. (1999-c).

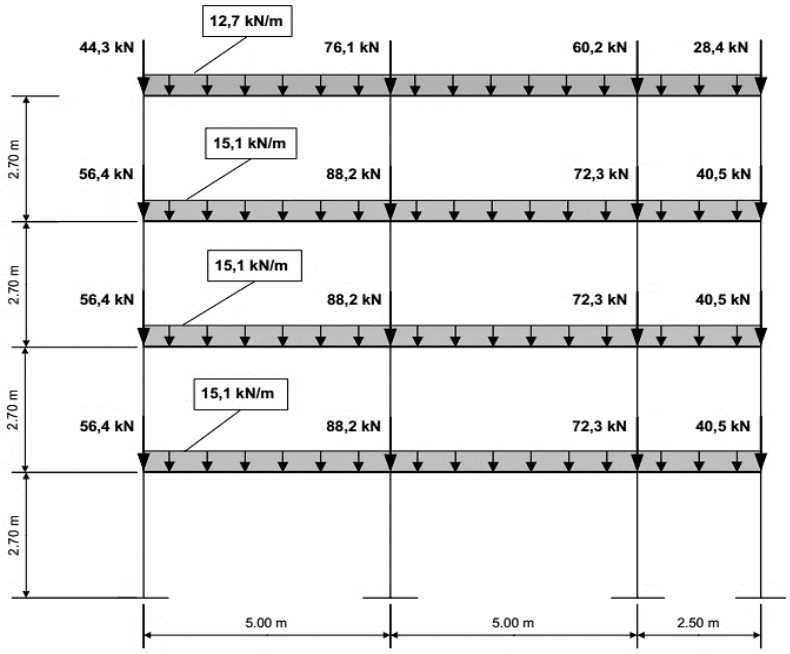

Figure 3. Scheme of vertical loads for nonlinear analysis [12]

3.1. Material Properties

3.1.1. Concrete Model

Mander et al. (1988) [32] have proposed a unified stress–strain approach for confined concrete applicable to both circular and rectangular shaped transverse reinforcement. The stress–strain model is illustrated in Figure 4 and f'_{cc} is based on an equation suggested by Popovic (1973) [33]. For a slow (quasi-static) strain rate and monotonic loading, the longitudinal compressive concrete stress is given by:

$$f = \frac{f'_{cc}\, xr}{r-1+x^r} \tag{6}$$

Where f'_{cc} is the compressive strength of confined concrete and x is a ratio of longitudinal compressive concrete strain (ε_c), r is the ratio of the concrete's initial modulus to the difference of the initial and secant moduli of elasticity. These parameters and their components are mathematically expressed by:

$$x = \frac{\varepsilon_c}{\varepsilon_{cc}} \tag{7}$$

$$\varepsilon_{cc} = \varepsilon_{c0}\left[1 + 5\left(\frac{f'_{cc}}{f'_{c0}} - 1\right)\right] \tag{8}$$

As suggested by Richart et al. (1928) [34], where f'_{cc} and ε_{c0}= the unconfined concrete strength and corresponding strain, respectively (generally ε_{c0}= 0.002 can be assumed), and;

$$r = \frac{E_c}{E_c - E_{sec}} \tag{9}$$

Where

$$E_c = 5000\sqrt{f'_{c0}}\ MPa \tag{10}$$

Is the tangent modulus of elasticity of the concrete (1 MPa = 145 psi), and

$$E_{sec} = \frac{f'_{cc}}{\varepsilon_{cc}} \tag{11}$$

The characteristic parameters are listed below:

f_c = 16300 kPa, f_t = 1900 kPa, ε_c = 0.002 m/m, E_c = 18975 MPa

3.1.2. Steel Model

The cyclic behavior of the steel bars is simulated using the classical Menegotto and Pinto (1973) [35] model with kinematic hardening (Figure 5) and possibility to take into account buckling by introducing a negative modulus slope in compression depending on the transverse steel reinforcement spacing. The monotonic behavior is defined through the initial Young's modulus (E_s), the plastic threshold ($\varepsilon_{sy}, \sigma_{sy}$), the ultimate strength and strain (ε_u, σ_u) and the yielding slope (E_h). The unloading and reloading process, is guided by analytic relations (Equations 12 to 15) corresponding to a set of curves ranging between the elastic and the yielding asymptotes.

$$\sigma^* = b\varepsilon^* + \left[\frac{1-b}{\left(1+(\varepsilon^*)^R\right)^{1/R}}\right] \tag{12}$$

Where

$$\sigma^* = \frac{\sigma_s - \sigma_r}{\sigma_0 - \sigma_r} \tag{13}$$

$$\varepsilon^* = \frac{\varepsilon_s - \varepsilon_r}{\varepsilon_0 - \varepsilon_r} \tag{14}$$

$$R = R_0 - \frac{A_i \xi}{A_j + \xi} \tag{15}$$

Tension: i = 1 and j = 2; Compression: i = 3 and j = 4.(σ_s, ε_s) is the studied point; (σ_0, ε_0) is the crossing point of the elastic and yielding slopes; (σ_r, ε_r) are the coordinates of the previous point of load reversion; b is the E_h/E_s ratio; R is a shape parameter; ξ is the ratio between the maximum reached strain during loading; , ε_0, , R_0, , A_i and , A_j are material constants that can be obtained from experimental results.

The Menegotto-Pinto steel model is employed for defining the steel material with the following properties:

E_s = 2.00E + 008 kPa, f_y = 343000 kPa, μ = 0.0024.

The materials considered at the design phase were a low strength concrete class C16/20 (CEN, 1991) and smooth

reinforcement steel class Fe B22 k (Italian standards). The latter refers to smooth bars with a yield stress of 235 MPa and ultimate strength of 365 MPa.

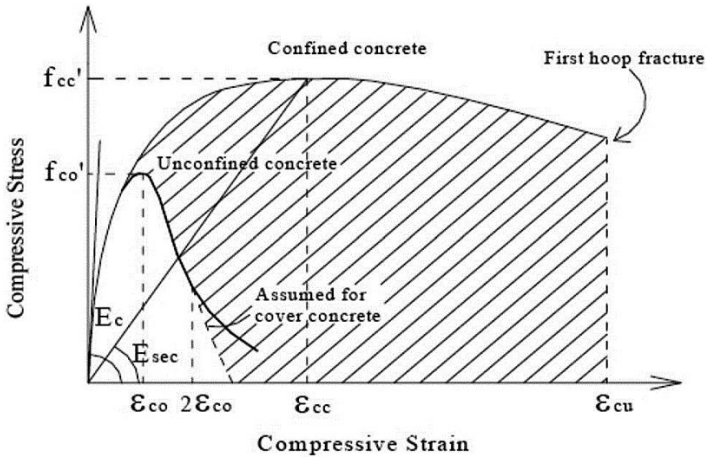

Figure 4. Mander et al. (1988) model for monotonic response of confined and unconfined concrete [32]

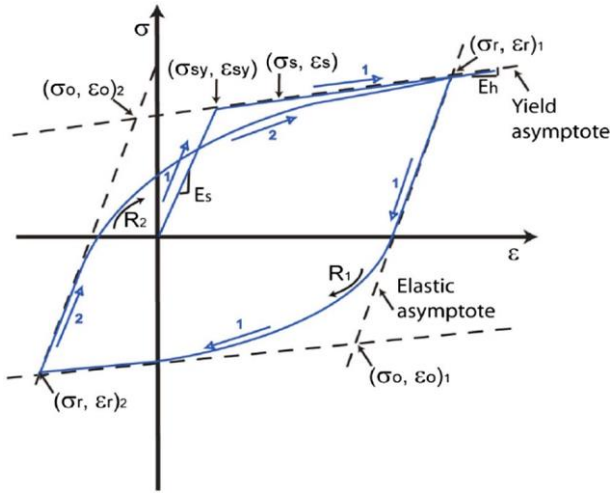

Figure 5. Steel model adapted from Menegotto and Pinto (1973) [35]

4. Earthquake Record Database

The seismic excitation consists of near-fault and far-fault earthquakes. In this study, the near-fault accelerograms database that it has been used here consists of 80 recorded ground-motion time histories from different fault types and damping ratio of 5% and earthquake magnitudes 5 < Ms < 8 that have occurred in the United States, Canada, Japan, Taiwan and Turkey. These accelerograms present peak ground acceleration (PGA) greater than or equal to 0.10g. These strong ground motions were recorded at stations where the closest to fault rupture is less than or equal to 20km. The complete list of these earthquakes, which were downloaded from the strong motion database of the Pacific Earthquake Engineering Research (PEER) [17] Center, is shown in Table 1 and Figure 6.

Near-fault seismic ground motions are frequently characterized by intense velocity and displacement pulses of relatively long period that clearly distinguish them from typical far-fault ground motions. Generally, forward directivity and permanent translation are the two main causes for the velocity pulses observed in near-fault regions [18].

A total of 80 real far-fault earthquake acceleration time histories from around the world are also used in this study. These accelerograms present maximum ground acceleration greater than or equal to 0.10g and are recorded at sites ranging from hard rock to soft soil conditions. The complete list of these earthquakes, which were also downloaded from the strong motion database of the PEER Center [17] is shown in Table 2 and Figure 7. On the other hand, Gillie et al. [19], Bray and Rodriguez-Marek [20], and Chopra and Chintanapakdee (2001) [7], suggest that Near-fault earthquakes (e.g. ED < 20 km) could have more devastating effects on structures that far-fault ones due to energy contents stored in relatively long-term pulses embedded in the ground motion.

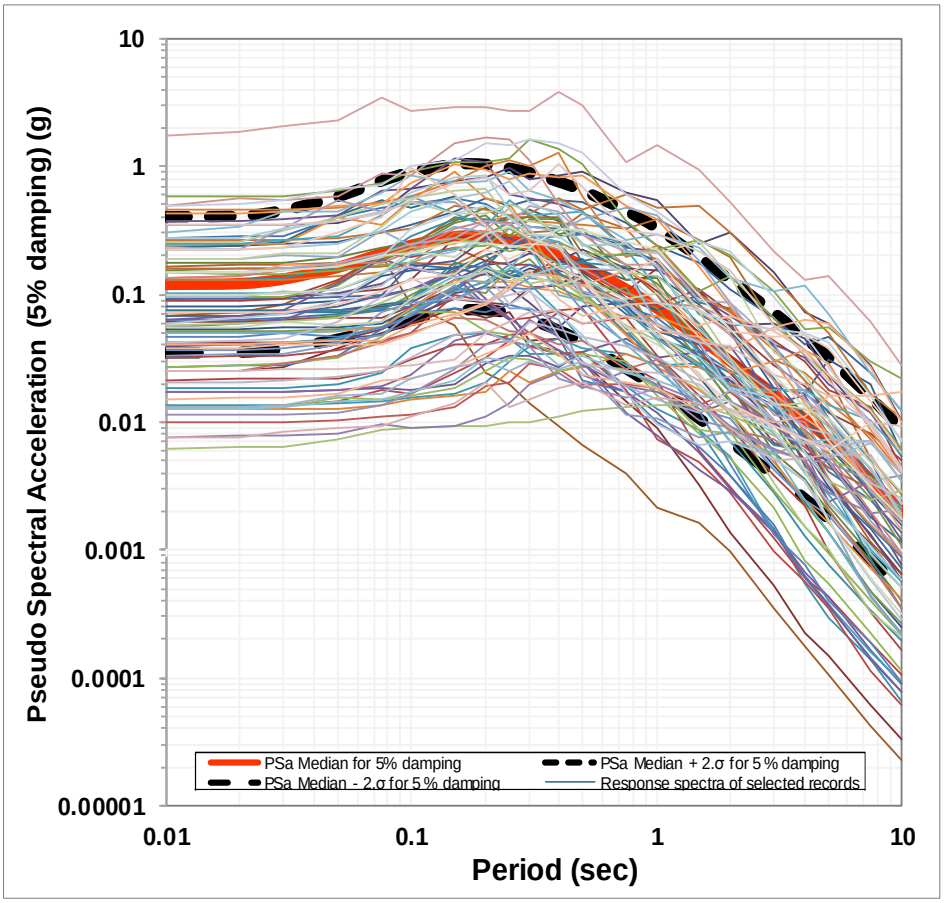

Figure 6. Response spectra of Near-fault ground motions used in this study

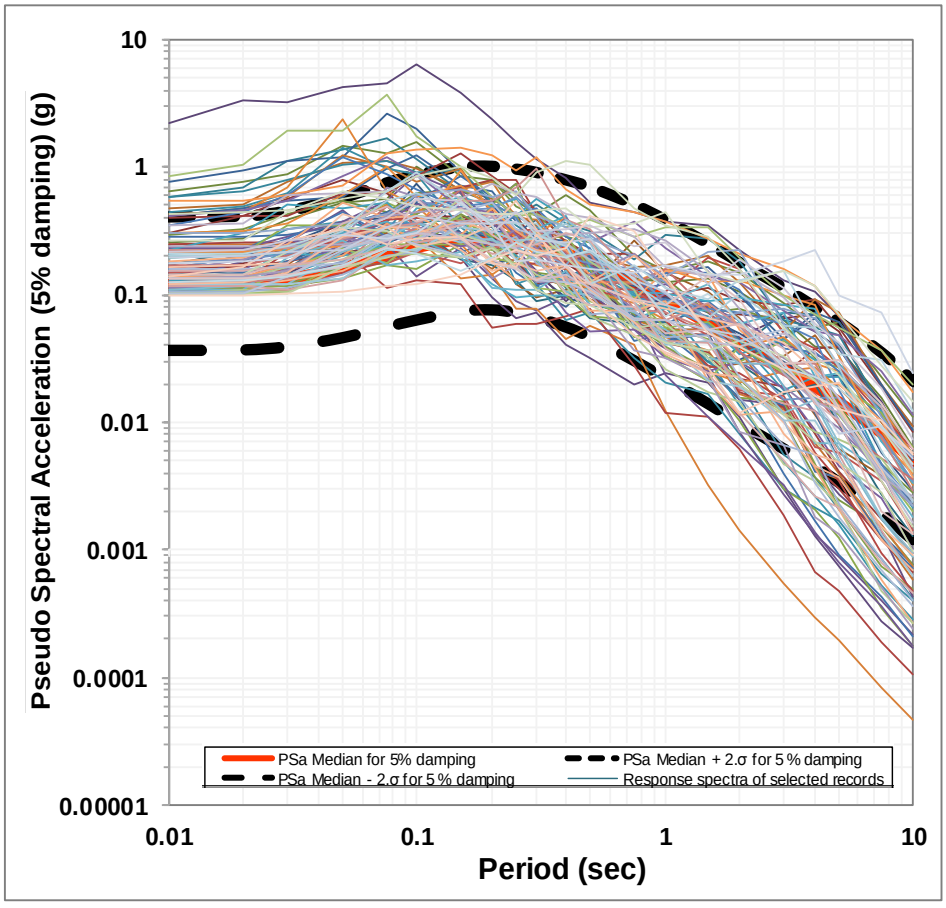

Figure 7. Response spectra of Far-fault ground motions used in this study

Table 1. Recorded near-fault ground motions used in this study

#	Earthquake	Magnitude	Epicentral Distance km	vs_{30} ms^{-1}	PGA g
1	Cape Mendocino, 25/04/1992, Cape Mendocino, 00	7.01	10.36	567.78	0.739
2	Cape Mendocino, 25/04/1992, Petrolia, 00	7.01	4.51	422.17	0.165
3	Chichi Taiwan,20/09/1999, TCU084, E	7.62	8.91	665.2	0.320
4	Chichi Taiwan,20/09/1999, WNT, EW	7.62	14.16	511.18	0.958
5	Chichi Taiwan,20/09/1999, TCU065, E	6.20	2.5	306	0.772
6	Chichi Taiwan,20/09/1999, TCU067, E	6.20	1.1	443.04	0.491
7	Chichi Taiwan,20/09/1999, TCU102, E	6.20	1.2	443.04	0.297
8	Coalinga-01,02/05/1983, Pleasant Valley,45	6.36	9.98	257.38	0.216
9	Coalinga-05,22/07/1983, Transmitter Hill, N	5.77	5.99	477.25	0.400
10	Coalinga-07,22/05/1983, Sulphur Baths, E	5.21	12.02	617.43	0.153
11	Coyote Lake,06/08/1979, Gilroy Array #1, E050W	5.74			0.132
12	Coyote Lake,06/08/1979, Gilroy Array #2	5.74	10.94	270.84	0.168
13	Coyote Lake,06/08/1979, Gilroy Array #4	5.74	7.67	221.78	0.422
14	Coyote Lake,06/08/1979, Gilroy Array #6	5.74	4.37	663.31	0.149
15	Duzce, Turkey,12/11/1999, Duzce, EW	7.14	1.61	281.86	0.346
16	Duzce, Turkey,12/11/1999, Lamont, NS	7.14	13.41	529.18	0.133
17	Erzican, Turkey,13/03/1992, Erzincan, NS	6.69	8.97	352.05	0.235
18	Imperial Valley-02, 19/05/1940, El Centro Array #9, 180	6.95	6.09	213.44	0.253
19	Imperial Valley-02, 19/05/1940, El Centro Array #9, 270	6.95			0.154
20	Imperial Valley-06,15/10/1979, Aeropuerto Mexicali, N Aeropuerto Mexicali	6.53	2.47	259.86	0.160
21	Imperial Valley-06,15/10/1979, Bonds Corner,140	6.53	6.19	223.03	0.532
22	Imperial Valley-06,15/10/1979, Chihuahua,12	6.53	18.88	242.05	0.216
23	Imperial Valley-06,15/10/1979, El Centro Array #6,140	6.53	19.44	264.57	0.249
24	Irpinia, Italy-01,23/11/1980, Sturno,00	6.90	10.80	382	0.319
25	Irpinia, Italy-01,23/11/1980, Calitri	6.90	15.04	455.93	0.170
26	Irpinia, Italy-02,23/11/1980, Calitri	6.20	11.97	455.93	0.158
27	Kobe, Japan,16/01/1995, KJMA, NS	6.90	18.27	312	0.339
28	Kobe, Japan,16/01/1995, Port Island (0 m)	6.90	19.25	198	0.567
29	Kobe, Japan,16/01/1995, Port Island (16 m)	6.90	13.12	256	0.284
30	Kobe, Japan,16/01/1995, Takatori, NS	6.90	19.25	0	0.806
31	Kobe, Japan,16/01/1995, Takarazuka, NS	6.90			0.693
32	Kobe, Japan,16/01/1995, Takarazuka, EW	6.90			0.694
33	Kocaeli, Turkey,17/08/1999, Izmit, 90	7.51	5.31	811	0.145
34	Kocaeli, Turkey,17/08/1999, Izmit, EW	7.51			0.220
35	Kocaeli, Turkey,17/08/1999, Yarimca,30	7.51	19.30	297	0.242
36	Kocaeli, Turkey,17/08/1999, Yarimca,60	7.51			0.349
37	Kocaeli, Turkey,17/08/1999, Sakarya, EW	7.51			0.376
38	Landers,28/06/1992, Joshua Tree	7.28	13.67	379.32	0.181
39	Landers,28/06/1992, Lucerne,260	7.28	2.19	1369	0.650
40	Landers,28/06/1992, Lucerne,345	7.28			0.613
41	Livermore,27/01/1980,57T01Livermore, EW	5.42	3.33	387.04	0.258
42	Livermore,27/01/1980,57T01Livermore, NS	5.42	10.33	550.88	0.233
43	Livermore,27/01/1980,57T02Livermore, EW Livermore,27/01/1980,57T01Livermore, NS	5.80	17.81	304.68	0.198
44	Livermore,27/01/1980,57T02Livermore, NS Livermore,27/01/1980,57T01Livermore, NS	5.80	16.66	384.47	0.252
45	Loma Prieta,18/10/1989, BRAN,00	6.93	9.01	476.54	0.506
46	Loma Prieta,18/10/1989, Corralitos, 00	6.93	7.17	462.24	0.458
47	Loma Prieta,18/10/1989, Corralitos, EW	6.93			0.479

48	Loma Prieta,18/10/1989, LGPC, NS	6.93	18.46	594.83	0.896
49	Loma Prieta,18/10/1989, LGPC, EW	6.93			0.605
50	Morgan Hill,24/04/1984, Anderson Dam, N070S	6.19	16.67	488.77	0.208
51	Morgan Hill,24/04/1984, Anderson Dam, E070W	6.19			0.423
52	Morgan Hill,24/04/1984, Halls Valley, N060S	6.19	3.94	281.61	0.156
53	Morgan Hill,24/04/1984, Halls Valley	6.19			0.312
54	N. Palm Springs,08/07/1986, Whitewater Trout Farm, NS	6.06	4.24	425.02	0.411
55	N. Palm Springs,08/07/1986, Whitewater Trout Farm, NS	6.06			0.612
56	Nahanni, Canada,23/12/1985, Site1	6.76	6.80	605.04	2.281
57	Nahanni, Canada,23/12/1985, Site1, N010S	6.76			0.978
58	Nahanni, Canada,23/12/1985, Site1, E010W	6.76			1.096
59	Nahanni, Canada,23/12/1985, Site2, N060S	6.76			0.489
60	Nahanni, Canada,23/12/1985, Site2, E060W	6.76			0.323
61	Northridge-01,17/01/1994, Arleta	6.69	11.10	297.71	0.552
62	Northridge-01,17/01/1994, Arleta, EW	6.69			0.344
63	Northridge-01,17/01/1994, LA - Sepulveda VA	6.69	8.48	380.06	0.318
64	Northridge-01,17/01/1994, LA - Sepulveda VA, EW	6.69			0.753
65	Northridge-01,17/01/1994, LA - Sepulveda VA, NS	6.69			0.939
66	Northridge-01,17/01/1994, Newhall	6.69	19.2	269.14	0.548
67	Northridge-01,17/01/1994, Rinaldi Receiving Sta Rinaldi Receiving Sta Rinaldi Receiving Sta	6.69	10.91	282.25	0.958
68	Northridge-01,17/01/1994, Sylmar - Converter Sta East	6.69	13.60	370.52	0.476
69	Northridge-01,17/01/1994, Sylmar - Olive View Med FF	6.69	16.77	440.54	0.536
70	Parkfield-02, CA,28/09/2004, Cholame 5W	6.00	13.76	236.59	0.184
71	Parkfield-02, CA,28/09/2004, Cholame 2E	6.00	12.06	522.74	0.202
72	Parkfield-02, CA,28/09/2004, Cholame 2WA	6.00	11.54	173.02	0.190
73	Parkfield,28/06/1966, Tamblor, N025S	6.00			0.357
74	Parkfield,28/06/1966, Tamblor, E025W	6.00			0.272
75	San Fernando, 9/2/1971, Pacoima Dam, N016S	6.61			1.226
76	San Fernando, 9/2/1971, Pacoima Dam, E016W	6.61			1.160
77	Superstition Hills-02,24/11/1987, Parachute Test Site,225	6.54	15.99	348.69	0.446
78	Superstition Hills-02,24/11/1987, Parachute Test Site,315	6.54	7.50	362.38	0.369
79	Superstition Hills-02,24/11/1987,Superstition Mnt, N045S	6.54			0.682
80	Superstition Hills-02,24/11/1987,Superstition Mnt,E045W	6.54			0.894

Table 2. Recorded Far-fault ground motions used in this study

#	Earthquake	Magnitude	Epicentral Distance km	vs_{30} ms^{-1}	PGA g
1	Lytle Greek,12/09/1970, Wrightwood, N115	5.22			0.162
2	Lytle Greek,12/09/1970, Wrightwood, N205	5.22			0.200
3	San Fernando, 9/2/1971, La Hollywoodstor,140	6.61	39.49	316.46	0.164
4	San Fernando, 9/2/1971, La Hollywoodstor,90	6.61	28.4		0.148
5	San Fernando, 9/2/1971, Lake Hughes #1,140	6.61	26.10	425.34	0.105
6	San Fernando, 9/2/1971, Lake Hughes #9, N069	6.61			0.154
7	San Fernando, 9/2/1971, Lake Hughes #9, N159	6.61			0.134
8	Friuli, Italy,15/09/1976, Forgaria Cornino, NS	5.90			0.212
9	Friuli, Italy,15/09/1976, Forgaria Cornino	5.90			0.260
10	Coyote Lake,06/08/1979, San Juan Bautista,255	5.74	23.24	335.5	0.117
11	Coyote Lake,06/08/1979, San Juan Bautista, N213	5.74	30.5		0.108

12	Coyote Lake,06/08/1979, San Juan Bautista, N303	5.74	30.5		0.107
13	Imperial Valley-06,15/10/1979, Delta,67	6.53	33.73	242.05	0.142
14	Imperial Valley-06,15/10/1979, El Centro Array #11,00	6.53	29.53	196.25	0.144
15	Imperial Valley-06,15/10/1979, El Centro Array #10,00	6.53	28.79	202.85	0.110
16	Imperial Valley-06,15/10/1979, El Centro Array #2,00	6.53	30.77	188.78	0.117
17	Imperial Valley-06,15/10/1979, EC County Center FF,160	6.53	29.07	192.05	0.245
18	Imperial Valley-06,15/10/1979, Brawley Airport,45	6.53	43.15	208.71	0.153
19	Livermore,27/01/1980, San Ramon, EW	5.90			0.301
20	Victoria, Mexico,09/06/1980, Cerro Prieto,00	6.33	33.73	471.53	0.292
21	Victoria, Mexico,09/06/1980, Cerro Prieto, N045	6.33			0.621
22	Victoria, Mexico,09/06/1980, Cerro Prieto, N135	6.33			0.587
23	Westmorland,26/04/1981, Westmorland Fire Sta, NS	5.90			0.368
24	Westmorland,26/04/1981, Westmorland Fire Sta, EW	5.90			0.496
25	Coalinga-01,02/05/1983, Parkfield, EW	6.36	32.19	467.76	0.147
26	Coalinga-01,02/05/1983, Parkfield, NS	6.36			0.131
27	Morgan Hill,24/04/1984, Gilroy Array #2	6.19	38.10	270.84	0.585
28	Morgan Hill,24/04/1984, Gilroy Array #3	6.19	38.20	349.85	0.403
29	Morgan Hill,24/04/1984, Gilroy Array #4	6.19	37.25	221.78	0.413
30	Morgan Hill,24/04/1984, Gilroy Array #6	6.19	36.34	663.31	0.406
31	Morgan Hill,24/04/1984, Gilroy Array #7	6.19	38.19	333.85	0.434
32	N. Palm Springs,08/07/1986, Cranston Forest Station	6.06	35.88	425.17	0.125
33	N. Palm Springs,08/07/1986, San Jacinto - Soboba	6.06	33.53	447.22	0.209
34	Whittier Narrows-01,04/10/1987, Mt Wilson - CIT Seis Sta	5.99	33.74	351.57	0.158
35	Whittier Narrows-01,04/10/1987, Mt Wilson - CIT Seis Sta	5.99			0.142
36	Superstition Hills-02,24/11/1987, El Centro Imp. Co. Cent	6.54	35.83	192.05	0.128
37	Superstition Hills-02,24/11/1987, El Centro Imp. Co. Cent	6.54			0.358
38	Superstition Hills-02,24/11/1987,salton sea wildlife Ref,45	6.54			0.119
39	Superstition Hills-02,24/11/1987,salton sea wildlife Ref,13	6.54			0.167
40	Superstition Hills-02,24/11/1987, Imperial Valley Wildlife Liquefaction Array	6.54	29.41	179	0.402
41	Loma Prieta,18/10/1989, Gilroy - Gavilan Coll	6.93	28.98	729.65	0.192
42	Loma Prieta,18/10/1989, Gilroy Array #1,	6.93	28.64	1428.14	0.215
43	Loma Prieta,18/10/1989, Gilroy Array #2	6.93	29.77	270.84	0.295
44	Loma Prieta,18/10/1989, Gilroy Array #3	6.93	31.40	349.85	0.342
45	Loma Prieta,18/10/1989, Gilroy Array #4	6.93	32.37	221.78	0.162
46	Loma Prieta,18/10/1989, Gilroy Array #6	6.93	35.47	663.31	0.102
47	Loma Prieta,18/10/1989, Gilroy Array #7	6.93	39.88	333.85	0.115
48	Loma Prieta,18/10/1989, Saratoga - Aloha Ave, NS	6.93	27.23	380.89	0.396
49	Loma Prieta,18/10/1989, Saratoga - Aloha Ave, EW	6.93			0.512
50	Loma Prieta,18/10/1989, Hollister City Hall, EW	6.93	47.90	198.77	0.217
51	Loma Prieta,18/10/1989, Hollister City Hall, NS	6.93			0.247
52	Cape Mendocino,25/04/1992, Rio Dell Overpass, EW	7.01	22.64	311.75	0.385
53	Cape Mendocino,25/04/1992, Rio Dell Overpass, NS	7.01			0.549
54	Cape Mendocino,25/04/1992, Centerville Beach, Naval Fac	7.01	28.01	459.04	0.122
55	Cape Mendocino,25/04/1992, Loleta Fire Station	7.01	35.31	515.65	0.123
56	Cape Mendocino,25/04/1992, Eureka, EW	7.01			0.178
57	Cape Mendocino,25/04/1992, Eureka, NS	7.01			0.154
58	Landers,26/06/1992, Coolwater	7.28	82.12	352.98	0.177
59	Landers,26/06/1992, Yermo Fire Station	7.28	85.99	353.63	0.136

60	Landers,26/06/1992, Joshua Tree, NS	7.28			0.284
61	Landers,26/06/1992, Joshua Tree, EW	7.28			0.274
62	Landers,26/06/1992, Amboy, NS Landers,26/06/1992, Joshua Tree, EW	7.28			0.115
63	Landers,26/06/1992, Amboy, EW	7.28			0.146
64	Northridge-01,17/01/1994, Canyon Country - W Lost, NS Cany	6.69	26.49	325.6	0.482
65	Northridge-01,17/01/1994, Canyon Country - W Lost, EW	6.69			0.410
66	Kobe, Japan,16/01/1995, Nishi-Akashi, NS	6.90			0.503
67	Kobe, Japan,16/01/1995, Nishi-Akashi, EW	6.90			0.509
68	Kobe, Japan,16/01/1995, Kakogawa, NS	6.90			0.345
69	Kocaeli, Turkey,17/08/1999, Duzce	7.51	98.22	281.86	0.206
70	Kocaeli, Turkey,17/08/1999, Gebze, NS	7.51			0.137
71	Kocaeli, Turkey,17/08/1999, Gebze, EW	7.51	47.03	792	0.244
72	Chi-Chi, Taiwan,20/09/1999, CHY101, E	7.62	31.96	258.89	0.166
73	Chi-Chi, Taiwan,20/09/1999, TCU045	7.62	77.50	704.64	0.356
74	Chi-Chi, Taiwan,20/09/1999, CHY041, E	7.62	51.15	492.26	0.125
75	Chi-Chi, Taiwan,20/09/1999, TCU095	7.62	95.70	446.63	0.256
76	Chi-Chi, Taiwan,20/09/1999,TAP003,EW	7.62			0.126
77	Chi-Chi, Taiwan,20/09/1999,TAP003,NS	7.62			0.106
78	Hector Mine,16/10/1999, Hector	7.13	26.53	726	0.149
79	Duzce, Turkey,12/11/1999, Bolu, NS	7.14	41.27		0.728
80	Duzce, Turkey,12/11/1999, Bolu, EW	7.14	41.27		0.822

5. Simulated Wind Field

In the present study, the wind field simulation is based on the algorithm suggested by Vanmarcke et al. (1993) [21] which consists of inferring correlated data series in a number of target points across a region bounded by a number of stations in which the characteristics of the random signal are known. This process is based on the best estimator of Fourier coefficients that can be used to reconstruct power spectra at the target locations which are consistent with realistic correlation laws such as those described by Dyrbye and Hansen (1997) and Simiu and Scanlan (1978) [22, 23]. The effectiveness of the method has been reported by a number of authors in the past, see for instance Gurley et al. (1997) [24], Martinez-Vazquez and Rodriguez-Cuevas (2007) [25], Martinez-Vazquez et al. (2010) [26]. Therefore, a brief explanation of the method together with some statistics of simulation results is provided below.

The simulation consisted of generating two uncorrelated time series that represent the wind regime of a suburb at heights of 10 and 250 m above the ground, using Monte Carlo techniques. These time series were taken as recorded data in the algorithm discussed in Vanmarcke et al. (1993) [21] from where partially correlated series at intermediate points could be inferred. The target turbulence intensity at z = 10 m was 0.295 and ~0.2 for the structures, respectively. The former being a standard value for suburban area whilst the latter was the value used in the experimental work reported in Melbourne (1980) and in Thordal et al. (2020) [27]. Table 1 shows the statistics of the simulated series located along the height of 250 for when the wind velocity at 10 m above the ground (U10) is 33 ms^{-1}.

In Table 3, U and σ^2 represent mean and variance of the series in ms^{-1} and m^2 s^{-2} whereas the subscripts represent target (t) and simulated (s) values, respectively. The mean square error between target and simulated values are of 4.7% for the mean velocity and 0. 9% for the variance. The target and simulated cross-correlation amongst time series is shown in Tables 4 and 5.

The mean square error of the correlation parameter is of 1.135% across all stations. This was considered acceptable and representative of wind events in suburban areas. A comparison between the simulated and theoretical wind power spectrum in the low frequency range is shown in Figure 8 for the position z = 10 m above the ground level.

The simulated power spectrum represents a single realisation and thus the spectral density fluctuates around the Von Karman spectrum. In Martinez-Vazquez and Rodriguez-Cuevas (2007) [25] and Martinez-Vazquez et al. (2010) [26], it is demonstrated that, by increasing the number of realisations, the ensemble of simulated spectral ordinates tends to theoretical values. For the purpose of the present study, the single realisation of the synthetic fields is considered to be appropriate [10].

Table 3. Calculated statistics of simulated wind time series [10]

Stats\z (m)	10	40	75	100	140	170	200	210	220	240	250
U_t	32.24	45.25	51.41	55.36	58.79	61.39	63.90	64.70	65.36	66.43	67.14
U_s	32.98	45.23	51.38	55.34	58.76	61.37	63.83	64.65	65.31	66.38	67.09
σ_t^2	94.77	86.89	78.77	71.39	63.26	55.88	47.59	44.72	42.26	38.03	35.08
σ_s^2	94.82	86.94	78.81	71.43	63.30	55.91	47.78	44.83	42.36	38.18	35.22

Table 4. Target cross-correlation [10]

	1	2	3	4	5	6	7	8	9	10	11
1	1.0000										
2	0.4237	1.0000									
3	0.2090	0.4767	1.0000								
4	0.1176	0.2605	0.5419	1.0000							
5	0.0653	0.1408	0.2895	0.5322	1.0000						
6	0.0394	0.0831	0.1690	0.3092	0.5798	1.0000					
7	0.0231	0.0479	0.0961	0.1748	0.3265	0.5625	1.0000				
8	0.0192	0.0394	0.0788	0.1429	0.2665	0.4588	0.8155	1.0000			
9	0.0164	0.0336	0.0669	0.1210	0.2255	0.3879	0.6893	0.8453	1.0000		
10	0.0127	0.0257	0.0508	0.0917	0.1705	0.2929	0.5200	0.6376	0.7543	1.0000	
11	0.0106	0.0213	0.0420	0.0756	0.1403	0.2408	0.4274	0.5240	0.6198	0.8217	1.0000

Table 5. Simulated cross-correlation [10]

	1	2	3	4	5	6	7	8	9	10	11
1	1.0000										
2	0.4737	1.0000									
3	0.4100	0.6224	1.0000								
4	0.2255	0.3814	0.6510	1.0000							
5	0.2134	0.2928	0.5322	0.7333	1.0000						
6	-0.0052	0.1594	0.2694	0.4118	0.6122	1.0000					
7	-0.0591	0.0892	0.2860	0.4189	0.5377	0.5934	1.0000				
8	-0.1249	0.0231	0.2238	0.3157	0.4465	0.5431	0.8046	1.0000			
9	-0.1843	-0.0493	0.1078	0.2204	0.3681	0.5346	0.7388	0.8113	1.0000		
10	-0.1688	-0.0151	0.1387	0.2723	0.3842	0.4584	0.6270	0.6355	0.7276	1.0000	
11	-0.0237	0.0716	0.2322	0.2803	0.3309	0.3253	0.5227	0.5248	0.5858	0.7524	1.0000

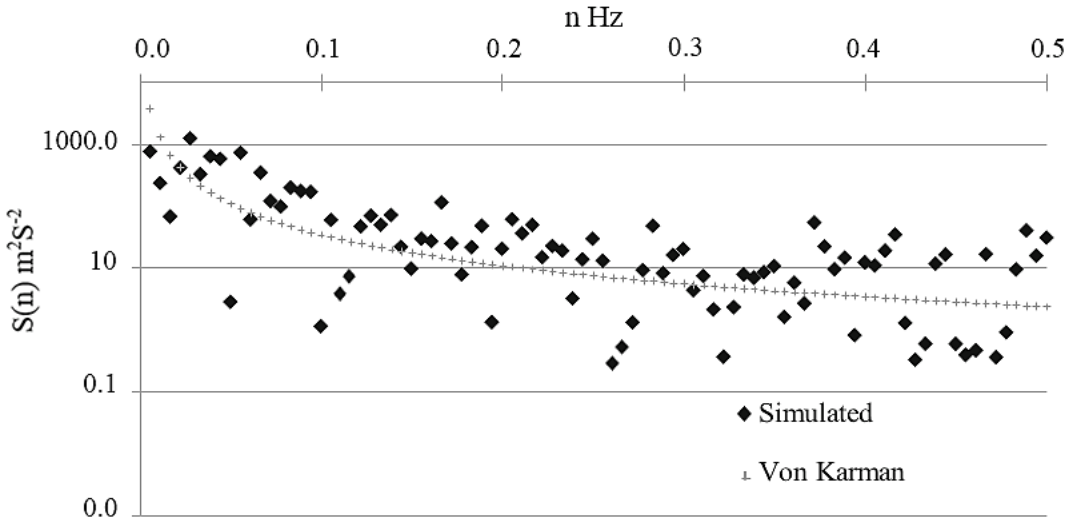

Figure 8. Simulated and theoretical wind power spectrum at 10 m above the ground

5.1. Dynamic Response

The static forces induced by wind were calculated using Equation 16. The reference height (z_r) was taken as of 10m.

$$F_i = \frac{1}{2}\rho C_D A_i U^2 \left(\frac{z}{z_r}\right)^{2\alpha} \quad (16)$$

Where ρ represents the density of air, C_D is a drag coefficient and A is the area exposed to wind. Whilst a value of α = 0.22 was used to represent the wind profile in suburban area.

6. Wind and Earthquake Loading

There is a fundamental difference between wind and earthquake load acting on large areas. The horizontal accelerations induced by earthquakes along the height of structures are assumed to be fully correlated by Chopra whereas the corresponding wind forces are not Dyrbye and Hansen (1997) [22]. The correlation of wind forces depends on the spatial distribution of wind gusts and that is usually taken into account through suitable correlation laws such as those proposed by Vickery (1970) [28] and Tanaka and Lawen (1986) [36] together with admittance functions such as that proposed by Davenport (1967) [29]. For point-like structure the input load can simply be obtained by superimposing both actions thus assuming these acts simultaneously whilst randomly off-phase [10].

7. Results and Discussion

After designing and detailing the reinforced concrete frame structure, the inelastic response of structure subject to earthquake and wind is performed by the nonlinear analysis software SeismoStruct 2016 [31]. Time history analysis is used to determine the maximum displacement response, and the Pushover analysis to obtain yield displacement of structure.

The pushover analysis consists of the application of gravity loads and a representative lateral load pattern. The lateral loads were applied monotonically in a step-by-step nonlinear static analysis. The applied lateral loads were accelerations in the x direction representing the forces that would be experienced by the structures when subjected to ground shaking. Under incrementally increasing loads some elements may yield sequentially. Consequently, at each event, the structures experience a stiffness change as shown in Figure 9, where IO, LS and CP stand for immediate occupancy, life safety and collapse prevention respectively. An elasto-plastic model for the above curves can be considered, so that the effect of this model would be equal to the effect of the real curve. In this method, drawing the complete elasto-plastic curve is based on the equalling of the structure energy absorption. It means that the area under the curve that indicates the amount of energy exerted to the structure should be equal in the elasto-plastic and the actual case. The yield point of the roof story can be obtained from these curves (Figure 9).

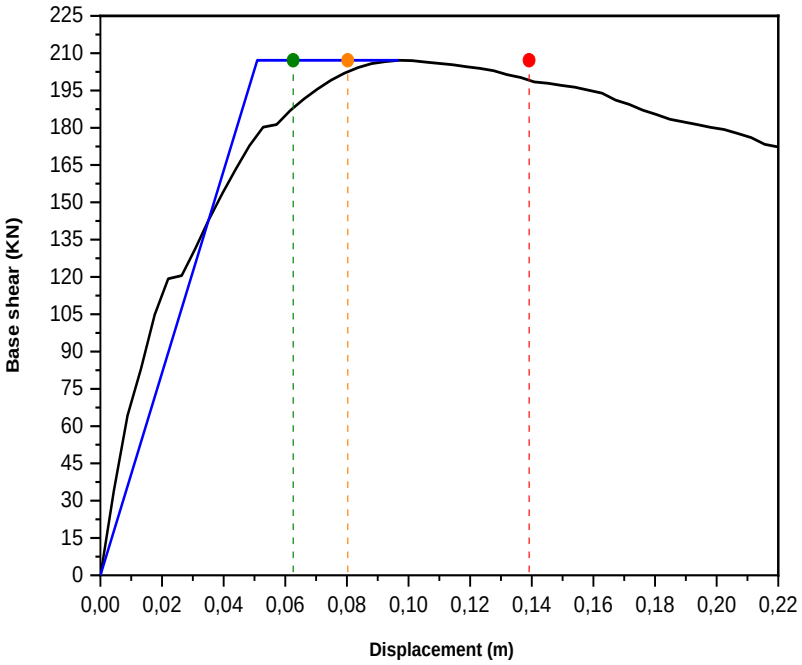

Figure 9. Pushover capacity curves for structure (● IO,● LS,● CP)

Table 6. Response of structure maximum values (summary table)

Base-shear (*kN*)		Top-displacement (*mm*)		Global damping (%)	
Seismo	exp.	Seismo	exp.	Seismo	exp.
207.13	209.0	50.9	60.8	7.8	8.5

7.1. Displacement, Base Shear and Ductility Demand-μ

In Figure 10a, the time histories (experimental results and numerical calculations) of top- displacement are plotted for Near-Fault input motion performed on the bare frame structure. Figure. 10b shows the top-displacement curves for Far-Fault earthquake, the comparisons between the experimental results and numerical results. The results are in good agreement for the first few second (< 7 s). Figure 11 presents the curves base-shear versus the period of the combined effect of earthquakes occurring simultaneously with the wind flowing.

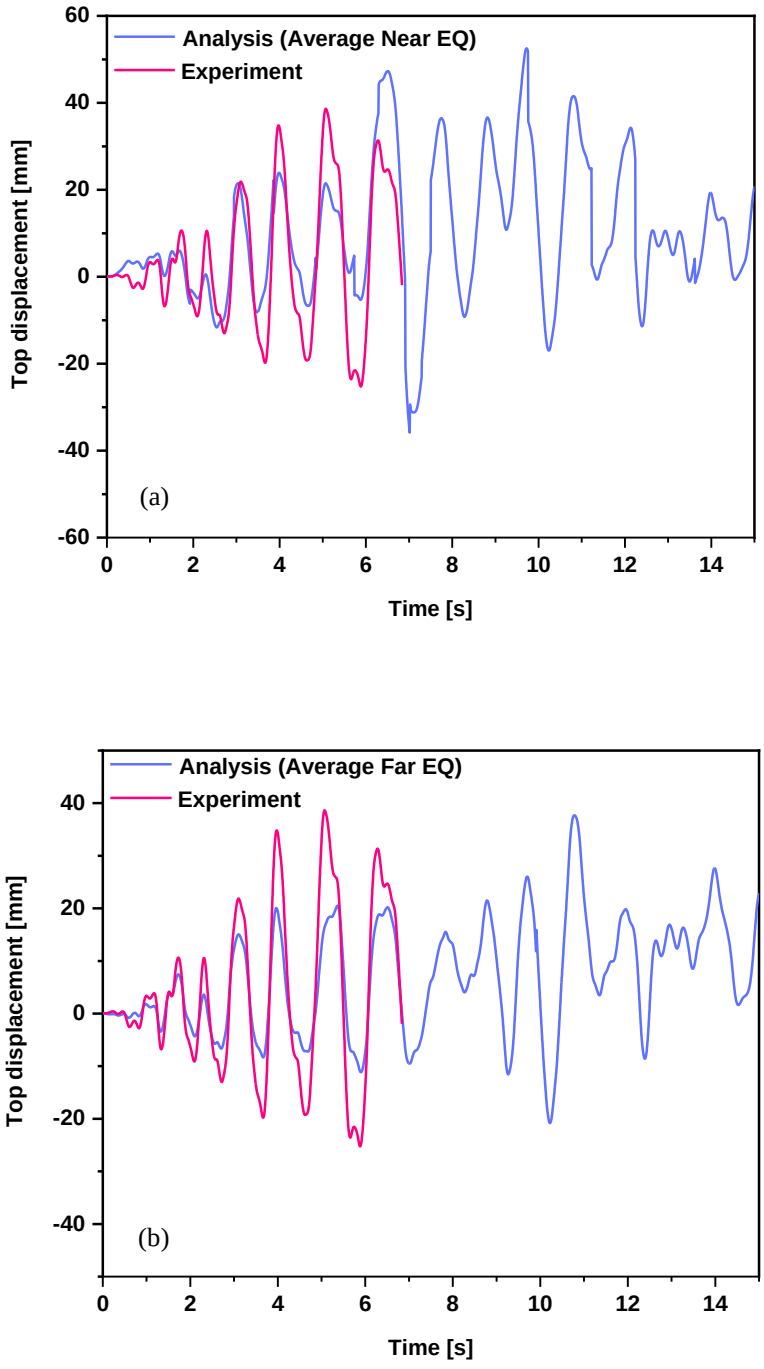

Figure 10. Experimental vs. Analytical results top displacement-time: (a) Average Near-fault EQ; (b) Far-fault EQ

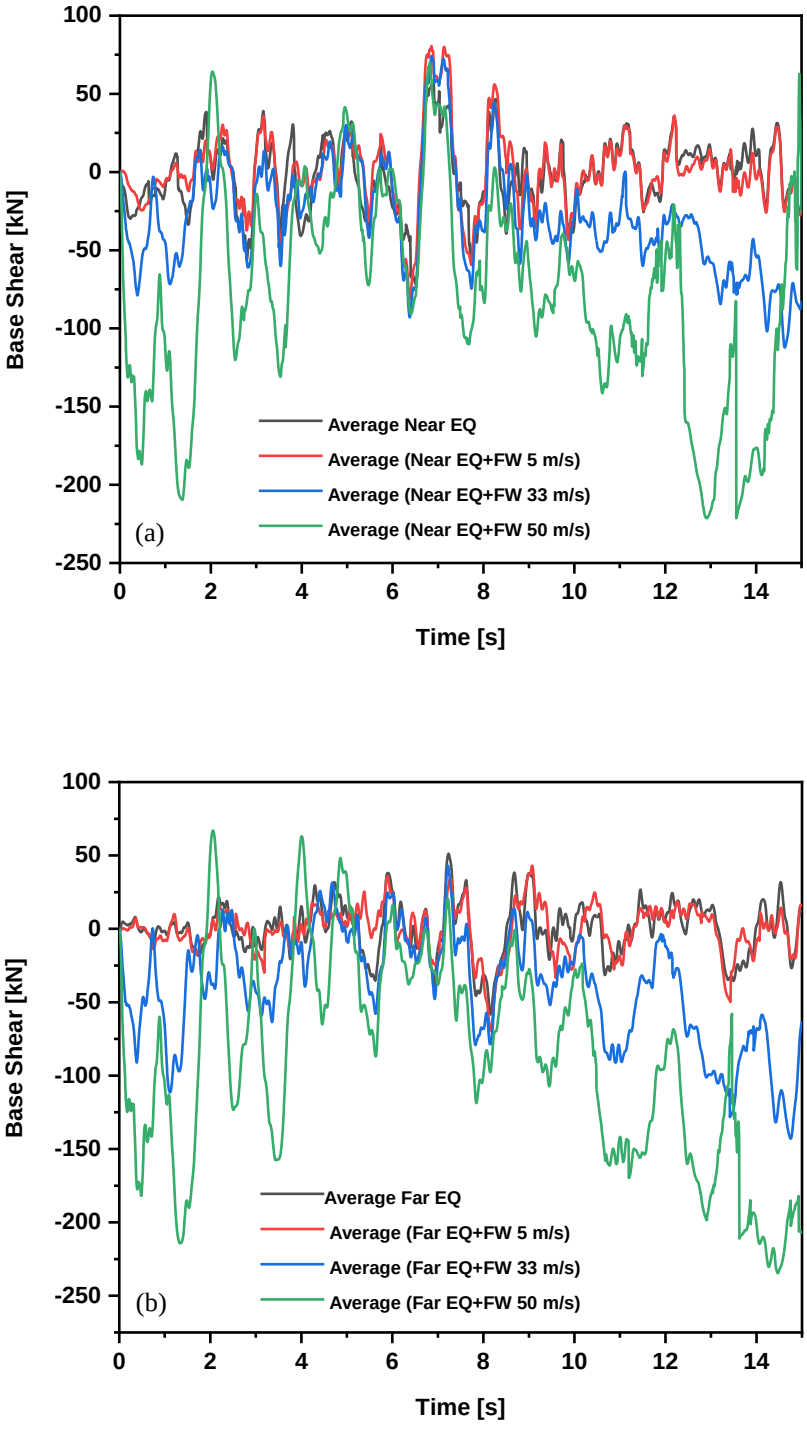

Figure 11. Analytical results–base shear-time: (a) Average Near-fault EQ + Force of wind; (b) Far-fault EQ + Force of wind

Figure 12 presents the average of ductility demand-μ for both the Near-fault and Far-fault sets. Looking at the results, it is concluded that the ductility-μ increases with wind velocity and therefore the influence of wind load on the inelastic response of structures increases with respect to that due to the sole action of earthquake load. At low wind velocity values (e.i velocity < 5 m/s) the ductility demand for Near-fault and Far-fault motions are approximate equivalent at zero wind speed. As the velocity of wind increases the ductility demand increases for short and intermediate wind speed. For the average of strength reduction factor show in Figure 13. Observe that a rapid increase in the interval $0 < T < 0.5$ followed by a change of direction into a region which tends to be flat until ~ $T = 3$ s.

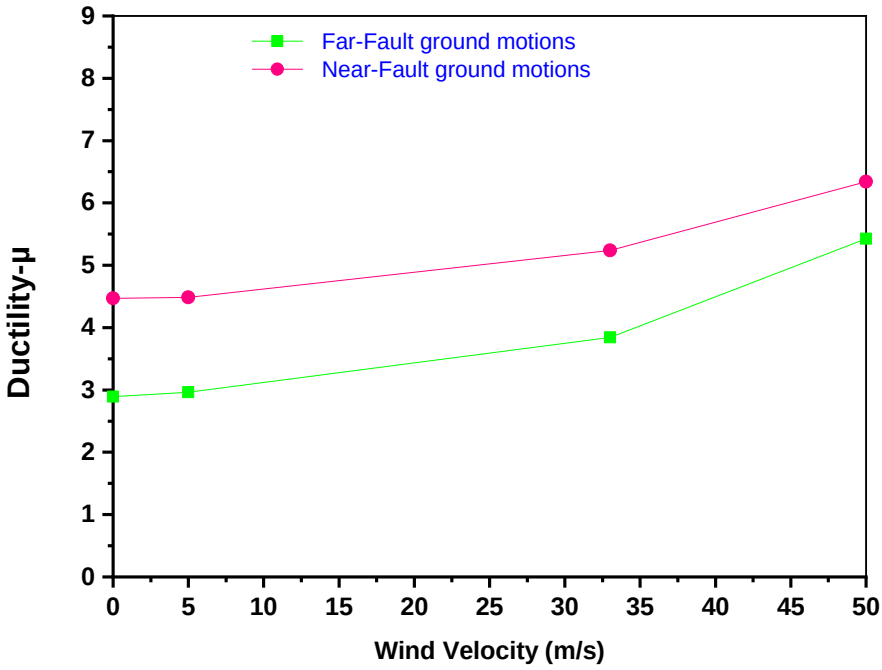

Figure 12. Ductility demand for Average Near-fault EQ and Far-fault EQ

The strength reduction factor depends not only on the characteristics of system, but also on the ground motion input. For given ground motion, R_μ is a function of the period of vibration T of structure, the damping the type of hysteretic behavior and the level of inelastic deformation studies reviewed in the previous section agree that for a given acceleration time history the strength reduction factor is primarily influenced by the period of vibration. Furthermore, Figure 13 show tow linear segments. In the first segment which corresponds to the short-period region, R_μ Increases linearly with increasing period from $R_\mu = 1$ to value that it is equal to ductility factor. In the second segment, the strength reduction factor maintains a constant value. The de details of the proposed relations depend on the hysteretic behavior and damping of system. This result coincides with comparisons of results in literature [29].

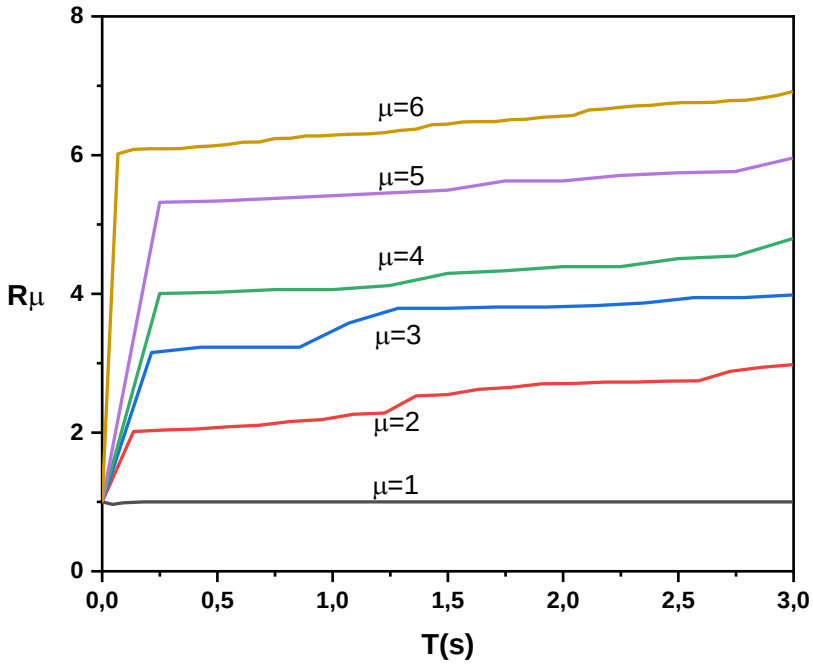

Figure 13. Strength reduction factor for Average Near-fault EQ and Far-fault EQ

8. Conclusion

This study presents ductility demands for Multi Degree Of Freedom (MDOF) systems under multiple near- and far-fault seismic ground motions. The main innovation of this work has to do with the influence of near- or far-fault earthquake commonly followed by a number of moderate to strong aftershocks and that wind is constantly flowing on ductility demands, a phenomenon which has not been studied in the past. This paper examines only and deals with the estimation of ductility demand (μ) and the strength reduction factor covering the combined effect of earthquakes occurring simultaneously with the wind flowing at mean speeds ranging between 5 and 50 ms^{-1}. This investigation shows the impact of considering wind load in the estimation of ductility demands. It is shown that ductility-μ increases with wind velocity and therefore the influence of wind load on the inelastic response of structures increases with respect to that due to the sole action of earthquake load. The estimated strength and ductility demand of wind simulated indicate that under certain conditions these can undergo unforeseen inelastic performance during extreme events. Furthermore, for given target ductility, the strength reduction factor can be exhibit great variations from one ground motion to another. For the design of a structure this means that the lateral strength capacity required to avoid displacement ductility demands larger than a given limit can have important variations from one ground motion to another. Finally, it is found that wind and earthquake combined effects strongly affects the ductility demand. This adds further arguments against current design assumptions which ignore multi-hazard scenarios. It seems therefore necessary to consider the risk to extreme events in the formulation of a more robust design framework for practical use.

9. Declarations

9.1. Data Availability Statement

The data presented in this study are available in article.

9.2. Funding

The author(s) received no financial support for the research, authorship, and/or publication of this article.

9.3. Acknowledgements

The present work has been developed at the school of Engineering of the University of Birmingham. I gratefully acknowledge the generous help and facilities of Birmingham University and many individuals, for their generous support. The Authors also acknowledges the reviewer suggestions made during the review phase of the publication.

9.4. Conflicts of Interest

The authors declare no conflict of interest.

10. References

[1] Park, Young-Ji, Alfredo H-S. Ang, and Yi Kwei Wen. "Seismic damage analysis of reinforced concrete buildings." Journal of Structural Engineering 111, no. 4 (1985): 740-757. doi:10.1061/(ASCE)0733-9445(1985)111:4(740).

[2] Yi, Wei-Jian, Hai-Yan Zhang, and Sashi K. Kunnath. "Probabilistic Constant-Strength Ductility Demand Spectra." Journal of Structural Engineering 133, no. 4 (April 2007): 567–575. doi:10.1061/(asce)0733-9445(2007)133:4(567).

[3] Hatzigeorgiou, George D., and Dimitri E. Beskos. "Inelastic Displacement Ratios for SDOF Structures Subjected to Repeated Earthquakes." Engineering Structures 31, no. 11 (November 2009): 2744–2755. doi:10.1016/j.engstruct.2009.07.002.

[4] Hatzigeorgiou, G.D. "Behavior Factors for Nonlinear Structures Subjected to Multiple Near-Fault Earthquakes." Computers & Structures 88, no. 5–6 (March 2010): 309–321. doi:10.1016/j.compstruc.2009.11.006.

[5] R.A. Medina, H. Krawinkler, "Seismic demands for non-deteriorating frame structures and their dependence on ground motions," Report no. 144. Stanford (CA), John A. Blume Earthquake Engineering Center, Department of Civil, Engineering, Stanford University, USA (2003).

[6] Ruiz-García, Jorge, and Eduardo Miranda. "Residual Displacement Ratios for Assessment of Existing Structures." Earthquake Engineering & Structural Dynamics 35, no. 3 (2006): 315–336. doi:10.1002/eqe.523.

[7] Chopra, Anil K., and Chatpan Chintanapakdee. "Comparing Response of SDOF Systems to Near-Fault and Far-Fault Earthquake Motions in the Context of Spectral Regions." Earthquake Engineering & Structural Dynamics 30, no. 12 (2001): 1769–1789. doi:10.1002/eqe.92.

[8] Amos, J. "Unsettled earth continues to rattle Nepal." BBC News-12 May (2015).

[9] Daniell, J. E., B. Khazai, F. Wenzel, and A. Vervaeck. "The CATDAT Damaging Earthquakes Database." Natural Hazards and Earth System Sciences 11, no. 8 (August 18, 2011): 2235–2251. doi:10.5194/nhess-11-2235-2011.

[10] Martinez-Vazquez, P. "Wind-Induced Vibrations of Structures Using Design Spectra." International Journal of Advanced Structural Engineering 8, no. 4 (October 31, 2016): 379–389. doi:10.1007/s40091-016-0139-4.

[11] Pinto, A., G. Verzeletti, J. Molina, H. Varum, R. Pinho, and E. Coelho. "Pseudo-dynamic tests on non-seismic resisting RC frames (bare and selective retrofit frames)." EUR Report 20244 (2002).

[12] Carvalho, E. C., Ema Coelho, and A. Campos-Costa. "Preparation of the full-scale tests on reinforced concrete frames-Characteristics of the test specimens, materials and testing conditions." ICONS report, Innovative Seismic Design Concepts for New and Existing Structures, European TMR Network-LNEC, Lisbon (1999).

[13] Miranda, Eduardo. "Site-Dependent Strength-Reduction Factors." Journal of Structural Engineering 119, no. 12 (December 1993): 3503-3519. doi:10.1061/(asce)0733-9445(1993)119:12(3503).

[14] Miranda, Eduardo, and Vitelmo V. Bertero. "Evaluation of Strength Reduction Factors for Earthquake-Resistant Design." Earthquake Spectra 10, no. 2 (May 1994): 357–379. doi:10.1193/1.1585778.

[15] Chopra, Anil K., and Rakesh K. Goel. "Capacity-Demand-Diagram Methods Based on Inelastic Design Spectrum." Earthquake Spectra 15, no. 4 (November 1999): 637–656. doi:10.1193/1.1586065.

[16] Riddell, Rafael, Jaime E. Garcia, and Eugenio Garces. "Inelastic Deformation Response of SDOF Systems Subjected to Earthquakes." Earthquake Engineering & Structural Dynamics 31, no. 3 (2002): 515–538. doi:10.1002/eqe.142.

[17] Pacific Earthquake Engineering Research Centre (PEER). PEER ground motion database. Available online: http://ngawest2.berkeley.edu/#disclaimer (accessed on March 2020).

[18] Mavroeidis, G. P. "A Mathematical Representation of Near-Fault Ground Motions." Bulletin of the Seismological Society of America 93, no. 3 (June 1, 2003): 1099–1131. doi:10.1785/0120020100.

[19] Gillie, Joanna L., Adrian Rodriguez-Marek, and Cole McDaniel. "Strength Reduction Factors for Near-Fault Forward-Directivity Ground Motions." Engineering Structures 32, no. 1 (January 2010): 273–285. doi:10.1016/j.engstruct.2009.09.014.

[20] Bray, Jonathan D., and Adrian Rodriguez-Marek. "Characterization of Forward-Directivity Ground Motions in the Near-Fault Region." Soil Dynamics and Earthquake Engineering 24, no. 11 (December 2004): 815–828. doi:10.1016/j.soildyn.2004.05.001.

[21] Vanmarcke, Erik H., Ernesto Heredia-Zavoni, and Gordon A. Fenton. "Conditional Simulation of Spatially Correlated Earthquake Ground Motion." Journal of Engineering Mechanics 119, no. 11 (November 1993): 2333-2352. doi:10.1061/(asce)0733-9399(1993)119:11(2333).

[22] Dyrbye, Claës, and Svend Ole Hansen. "Wind loads on structures." (1997).

[23] Simiu E, Scanlan H. "Wind effects on structures: an introduction to wind engineering." University of Michigan (1978): 589.

[24] Gurley, Kurtis R., Michael A. Tognarelli, and Ahsan Kareem. "Analysis and Simulation Tools for Wind Engineering." Probabilistic Engineering Mechanics 12, no. 1 (January 1997): 9–31. doi:10.1016/s0266-8920(96)00010-0.

[25] Martínez-Vázquez, Pedro, and Neftalí Rodríguez-Cuevas. "Wind Field Reproduction Using Neural Networks and Conditional Simulation." Engineering Structures 29, no. 7 (July 2007): 1442–1449. doi:10.1016/j.engstruct.2006.08.024.

[26] Martinez-Vazquez, P., C.J. Baker, M. Sterling, A. Quinn, and P.J. Richards. "Aerodynamic Forces on Fixed and Rotating Plates." Wind and Structures an International Journal 13, no. 2 (March 25, 2010): 127–144. doi:10.12989/was.2010.13.2.127.

[27] Thordal, Marie Skytte, Jens Chr Bennetsen, Stefano Capra, and H. Holger H. Koss. "Towards a Standard CFD Setup for Wind Load Assessment of High-Rise Buildings: Part 1 – Benchmark of the CAARC Building." Journal of Wind Engineering and Industrial Aerodynamics 205 (October 2020): 104283. doi:10.1016/j.jweia.2020.104283.

[28] Vickery B J. "On the reliability of gust loading factors. Proc. Technical Meeting Concerning Wind Loads on Buildings and Structures." Build. Sc. Ser. 30. Ntl. Bureau of Standards, Washington DC, (1970): 93-104.

[29] Davenport, Alan G. "Gust Loading Factors." Journal of the Structural Division 93, no. 3 (March 1967): 11–34. doi:10.1061/jsdeag.0001692.

[30] Tena-Colunga, A. "Displacement ductility demand spectra for the seismic evaluation of structures." Engineering Structures 23, no. 10 (2001): 1319-1330. doi: 10.1016/S0141-0296(01)00025-6.

[31] SeismoSoft, SeismoStruct. "A computer program for static and dynamic nonlinear analysis of framed structures," (2016) Available online: https://seismosoft.com/wp-content/uploads/prods/lib/SeismoStruct-2021-User-Manual_ENG.pdf (accessed on December 2020).

[32] Mander, J. B., M. J. N. Priestley, and R. Park. "Theoretical Stress ‐ Strain Model for Confined Concrete." Journal of Structural Engineering 114, no. 8 (September 1988): 1804 ‐ 1826. doi:10.1061/(asce)0733-9445(1988)114:8(1804).

[33] Popovics, Sandor. "A Numerical Approach to the Complete Stress-Strain Curve of Concrete." Cement and Concrete Research 3, no. 5 (September 1973): 583–599. doi:10.1016/0008-8846(73)90096-3.

[34] Richart, Frank Erwin, Anton Brandtzæg, and Rex Lenoi Brown. "A study of the failure of concrete under combined compressive stresses." University of Illinois at Urbana Champaign, College of Engineering. Engineering Experiment Station, (1928).

[35] Menegotto, Marco., and P.E. Pinto "Method of analysis for cyclically loaded RC plane frames including changes in geometry and non-elastic behavior of elements under combined normal force and bending." In Proc. of IABSE symposium on resistance and ultimate deformability of structures acted on by well-defined repeated loads, (1973): 15-22.

[36] Tanaka, H., and N. Lawen. "Test on the CAARC standard tall building model with a length scale of 1: 1000." Journal of wind engineering and industrial aerodynamics 25, no. 1 (1986): 15-29.